IOP Conf. Series: Materials Science and Engineering **655** (2019) 012012 doi:10.1088/1757-899X/655/1/012012

Carbide-free bainitic steels for rail wheel applications

A Kapito[1,2], R J Mostert[2], W E Stumpf[2] and C W Siyasiya[2]

1. Advanced Materials Division, Mintek, 200 Malibongwe Drive, Randburg, 2125, South Africa

2. Department of Materials Science and Metallurgical Engineering, University of Pretoria, South Africa

E-Mail: asimenyek@mintek.co.za[a]

Abstract: In South Africa, forged wheels for rail cars are imported but cast wheels are manufactured locally, although recent developments indicate that forged wheels will in future be manufactured locally. The forged wheels are generally manufactured from AAR Class C steel, which is a high carbon, pearlitic steel used for rail application. Railway wheels are a costly component of the railway wagon as they experience wear and damage during application. Improvements in the mechanical properties are thus desired. Against this background, a project is reported on the development of durable rail steel alloys for railway wheel applications.
Carbide-free bainite is a novel microstructure comprising bainitic ferrite and retained austenite/martensite but without coarse carbides in the interlath positions. The absence of carbides is achieved through the addition of a high silicon (~2wt%) content to the steel. This carbide-free bainite can achieve high tensile strength (>1000MPa) and toughness (40J, 20°C) as well as good wear resistance. These alloys have found application in areas where high strength, toughness and wear resistance are required, such as in rail steels, and have been deemed the "next generation" of rail steels.
Carbide-free experimental alloys were produced in the laboratory and tested for mechanical properties such as hardness, tensile strength and impact toughness. The properties of the laboratory alloys were compared to those of standard Class C alloys used in South Africa to determine their potential use as railway wheel alloys.

1. Introduction

1.1. Pearlitic Steels for Rail Applications

Rail steels are generally made of medium and high-carbon steel with a pearlitic microstructure (Figure 1). The alternating plates, or lamella, of cementite and ferrite are ideal for the type of operating conditions experienced during rail transport [1],[2]. Solid wheel steel grades for heavy haul are mainly governed by the Association of American Railroad's (AAR) standards [3], [4] and the main steel grades particularly recommended for heavy haul are the medium-high carbon pearlitic steels [3], [4].

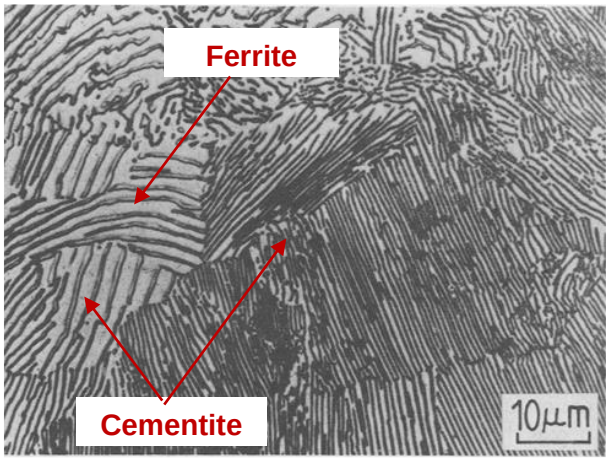

Figure 1. Microstructure of pearlite, a lamellar mixture of ferrite and cementite [1].

To extend the life cycle of rail steels, hardness has traditionally been the primary property to exploit, see Figures 2 and 3 [2]. Figure 2 shows the historical development of rail steels and it is clear that the tensile strength of the rail steels has increased continuously over the years [8]. This is mainly due to an increase in the hardness of the steel, to reduce the wear rate, and also due to the development of technologies in the steel-making process [8]. In Figure 2, R200, R260, R320Cr and R350HT are names for pearlitic rail steels grades, developed over the years, with Brinell hardness of 200BHN, 260BHN, 320BHN and 350BHN respectively. Figure 2 also shows the steel named Dobain®, a specially heat-treated bainitic high-grade steel developed in Europe in the 2000's for rail steel applications.
The hardness of a pearlitic rail steel is increased by decreasing the interlamellar spacing and increasing the content of alloying elements, such as manganese and chromium but particularly carbon [2]. Figure 3 shows that a fine pearlitic spacing results in a steel with a higher hardness and yield strength [5]. Therefore the shorter the interlamellar spacing, the better the mechanical properties of the rail steel.

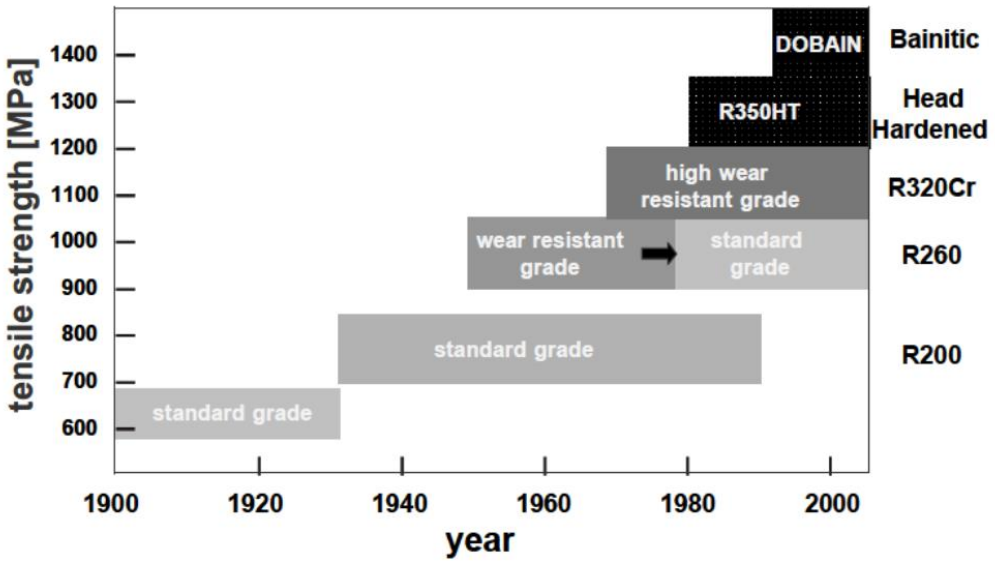

Figure 2. Trends in the development of rail steels from the 1900's to 2000's showing the different grades of steel developed with an increase in tensile strength and hardness [8].

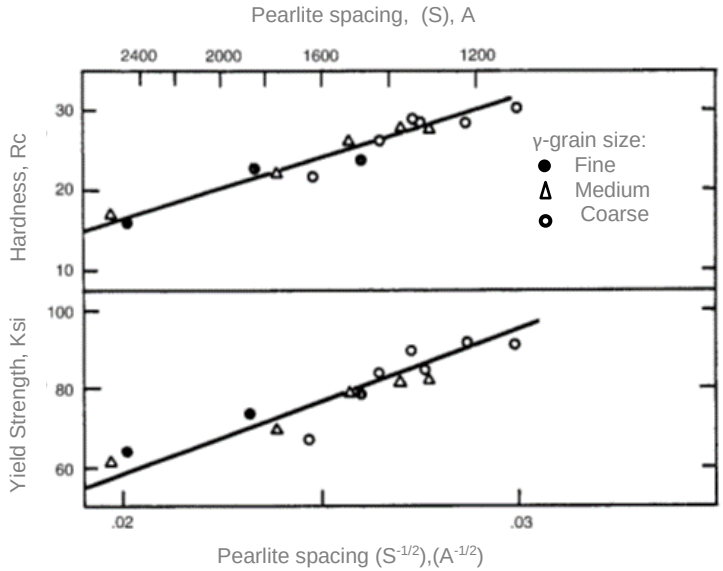

Figure 3. Hardness and yield strength as a function of pearlite interlamellar spacing in a fully pearlitic microstructures [5].

1.2. The Minimum Pearlite Interlamellar Spacing (d)

Pearlite grows in a lamellar structure with the pearlite spacing (d) defined as the perpendicular distance across two consecutive lamellae [6], [7]. Interlamellar spacing is generally measured using the scanning electron microscope (SEM) or the transmission electron microscope (TEM), except if it is very coarse and optical microscopy can be used [7]. The minimum pearlite spacing that can be achieved after transformation from austenite has a thermodynamic relationship as indicated in equation 1:

$$d_{\min} = -\frac{2\gamma_{SF}}{\Delta H_v} \times \frac{1}{\Delta T}. \quad [6] \qquad \textit{Equation 1}$$

Where γ_{SF} = surface energy of the Fe_3C/α interface and ΔH_v = change in enthalpy and $\Delta T = T - T_e$ (the undercooling below the eutectic temperature and T = transformation temperature and T_e is the eutectoid temperature) [6].

The minimum pearlite spacing decreases with a decrease in transformation temperature. The actual pearlite spacing that is achievable by the current production methods is very close to the theoretical d_{min}. Experimentally the actual spacing will always be greater than the theoretical minimum. This limits the further development of pearlitic steels with shorter pearlitic spacings. This has led to the search of alternative rail microstructures such as bainite.

2. Carbide-Free Bainitic Steels

Bainitic steels inherently have better toughness, ductility and weldability than the conventional pearlitic steels. Most modern bainitic steels are designed with much reduced carbon and other alloying elements to form lean alloys [9]. The reduced alloy concentration gives better weldability and improved toughness. The conventional bainitic steels have coarse interlath carbides and generally have poorer toughness and wear resistance than the pearlitic rail steels. This has focused attention on the development of carbide-free bainitic steels.

In the recent decades, Bhadeshia *et al* have developed and introduced high silicon, high carbon bainitic steels [10]-[16]. It is known that the precipitation of cementite during bainitic transformation can be suppressed by alloying the steel with about 1.5 wt% of silicon [10]-[15]. An interesting microstructure results when this silicon–alloyed steel is transformed into upper bainite. The carbon that is rejected into the residual austenite, instead of precipitating as interlath cementite, remains in the austenite and stabilises it down to ambient temperature. The resulting microstructure consists of fine plates of bainitic

ferrite separated by carbon–enriched regions of austenite, see Figure 4 [11]. This microstructure is called carbide-free bainite.

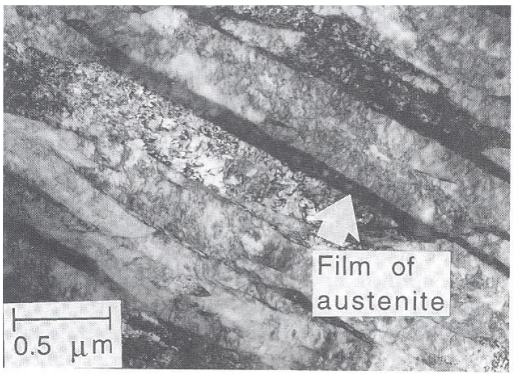

Figure 4. Transmission electron micrograph of a mixture of bainitic ferrite and stable austenite [11].

The alloying elements used to produce this microstructure are common to steel production, i.e. carbon, manganese, boron, etc. with particular addition of a high silicon content to supress cementite formation. The carbide-free bainitic steels have better fatigue properties than the pearlitic steels, accommodating longer crack lengths and growth rates before fracture. They also exhibit higher strength.
A number of carbide-free bainitic steels have thus been developed for rail applications [17], [18]-[35]. There is a government push to shift South Africa's freight transport from road to rail, cutting both high logistical costs and carbon emissions. This will require longer lasting railway components, such as wheels, to take up the higher load. In South Africa, rail AAR Class C forged wheels are used for heavy haul transportation. Durable wheel alloys would cut the maintenance costs of the railway industry significantly. In this study the carbide-free bainitic alloys were explored as possible alternatives for forged rail wheel applications.

3. Experimental Procedure

Melting was done at 1650°C in an induction melting furnace and casting, in air, using a 150 kg alumina crucible, into a designed sand mould. Aluminium (0.2 wt%) was added to the melt for deoxidation. After casting the ingots were allowed to air cool in the moulds. After cooling, the moulds were broken and the ingots (45 mm thickness) were hot forged and hot rolled at 900 °C into 15 mm thick plates, sufficient thickness for the production of the tensile and impact specimens. Chemical composition analysis was conducted using spark emission spectrometry and hardness using Vickers hardness testing (load of 200g, dwell time of 15s). For Micro-Vickers the load used for 30g for a dwell time also of 15s. Neutron diffraction was conducted to measure the retained austenite in the experimental alloys. Optical microscopy and transmission Kikuchi diffraction (TKD) was used to analyse the microstructures of the alloys. Tensile testing was conducted according to ASTM E8 and impact testing according to ASTM E23.

4. Results

4.1. Chemical Composition

Four Alloys E to H with variations in silicon content, were manufactured to study their tensile and impact properties. Table 1 gives the chemical compositions of the experimental alloys. The chemical composition of the four alloys comprised typical alloying elements used to produce rail steels, but with a high silicon content of 1-2 wt% used to retard the formation of cementite in the steel. Alloy E with a low silicon content of 0.36 wt% was produced as a reference alloy, to determine if this low silicon content will produce carbides in the microstructure. The results are an average of three readings.

Table 1. Chemical composition of experimental Alloys E to H, wt%

Alloy	C	Si	Mn	P	S	Cr	Mo	Al	B
E	0.19	0.36	1.41	0.017	0.009	0.5	0.26	0.003	0.0003
F	0.26	1.85	1.37	0.018	0.010	0.6	0.18	0.009	0.0007
G	0.29	1.47	1.38	0.016	0.011	0.5	0.17	0.018	0.0008
H	0.28	1.00	1.57	0.024	0.012	0.5	0.23	0.006	0.0003

4.2. Heat Treatment

The martensite start (M_s) and bainite start (B_s) temperatures for alloys E to H were calculated using well-known empirical equations as shown below, see Table 2 [6].

$M_s = 539 - 423C - 30.4Mn - 17.7Ni - 12.1Cr - 11.0Si - 7.0Mo$

$B_s = 630 - 45Mn - 40V - 35Si - 30Cr - 25Mo - 20Ni - 15W.$

The transformation temperatures (T_1) used to isothermally heat treat the alloys were chosen to be ~10°C above the M_s temperature, to maximise the volume fraction of bainite produced. The alloys were austenitised at temperatures T_A, which was ~50°C above the A_{C3} temperature and then quenched into a salt bath to a temperature T_1 to form bainite. The alloys were soaked for about an hour in the salt bath and then water quenched. Previous testwork was conducted to determine the time required in a salt bath for bainite formation and from these results it was found than an hour was enough to produce bainite in 15mm thick samples.

Table 2. The heat treatment temperatures for alloys E to H.

	Calculated °C		Calculated °C	Transformation °C	
Alloy	**M_s**	**B_s**	**A_{C3}**	**T_A**	**T_1**
E	405	594	836	900	415
F	367	583	844	900	380
G	355	577	835	900	365
H	356	555	830	900	370

4.3. The Microstructures of Alloys E to H

Figures 5 and 6 shows the microstructures attained for Alloys E to H, after heat treatment, comprising predominantly bainite (B) with some patches of martensite (M).

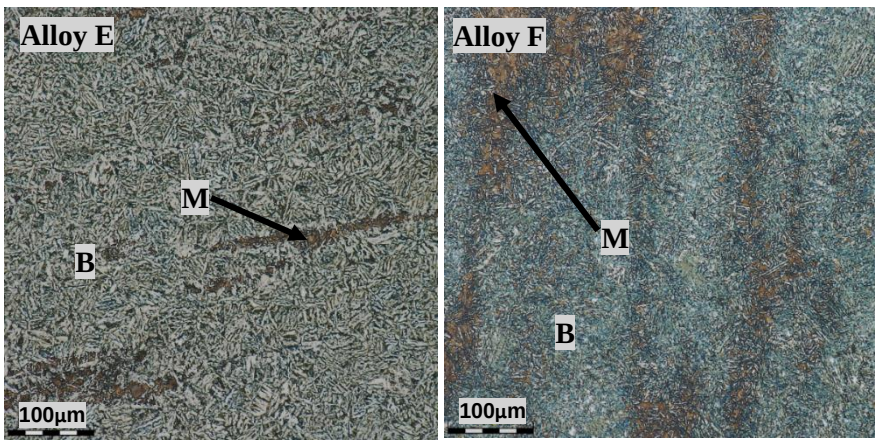

Figure 5. Microstructures of Alloys E and F showing bainite (B) and martensite (M).

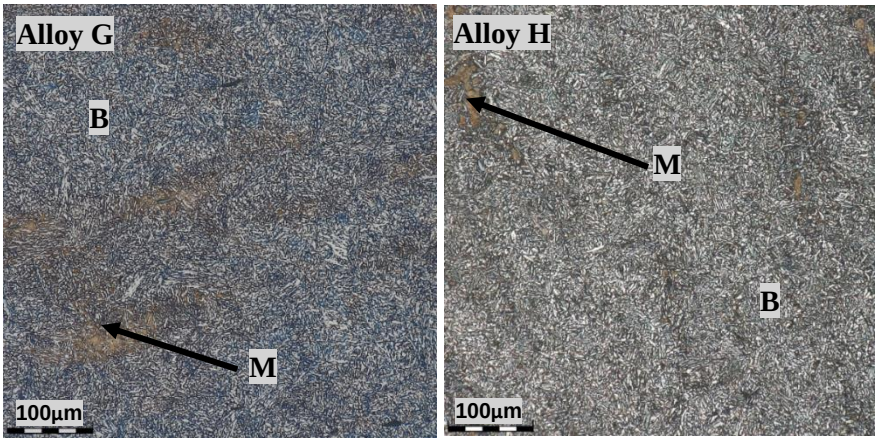

Figure 6. Microstructures of Alloys G and H showing bainite (B) and martensite (M).

To determine the volume fraction of the bainite, retained austenite and martensite in the microstructures of the alloys E to H, point counting and neutron diffraction were used, see Table 3. From the point counting it can be seen that the alloys have a high volume fraction of the bainite (B) phase, i.e. between 87%-98%. Only the martensite and bainite phases were counted using the point counting method. Neutron diffraction measured the retained austenite for alloy E (which had the lowest silicon content) to be 2.6%. Alloys F and H had high retained austenite contents of 20% and 25% respectively and alloy G had a retained austenite content of 9%. The average Vickers hardness of the alloys is also shown here together with the micro-Vickers hardness of the martensitic phase.

Table 3. Point counting, neutron diffraction and hardness measurements for alloys E to H, M = martensite and B = bainite, FCC = austenite, BCC = ferrite (a=b=c= 0.287)

	Point Counting		**Neutron Diffraction**		**Hardness (Hv)**	
Alloy	**M**	**B**	**BCC**	**FCC**	**Average**	**Micro-Vickers (Martensite Phase)**
E	12	88	97.4	2.6	284±6	498±8
F	13	87	80.0	20.0	412±41	503±3
G	2	98	90.6	9.4	352±7	296±6
H	10	90	74.5	25.5	295±2	467±9

4.4. Transmission Kikuchi Diffraction (TKD) for alloys E to H

TKD results for alloys E to H are given in Figures 7. The microstructure of alloy E, with a low silicon content of 0.3 wt%, showed evidence of cementite (yellow phase) in the microstructure along the boundaries of the bainite plates. Alloys F to H showed a microstructure of bainite and retained austenite with no cementite.

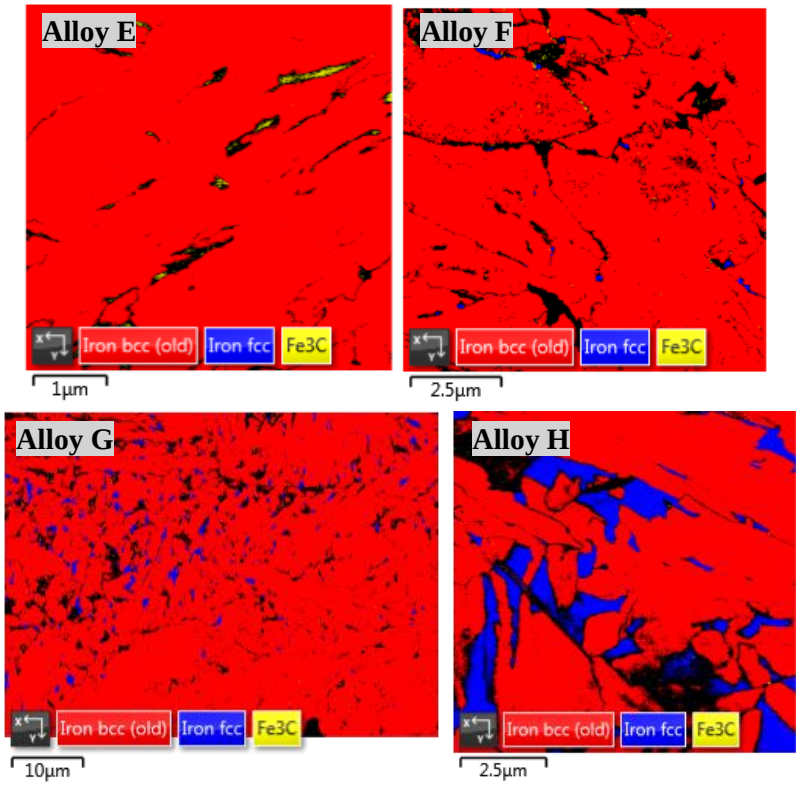

Figure 7. TKD micrographs of experimental bainitic alloys E to H showing FCC-austenite (blue) and BCC-ferrite (red phases). The black area is not a phase but regions in the sample that were not well resolved. 'old' refers to an old file name used to save the micrographs.

4.5. Tensile Tests

Rail wheels experience rolling contact fatigue and it is known that a high yield and tensile strength improves the rolling contact fatigue resistance of rail steels [8][22][31]. Table 4 shows the tensile test results conducted on alloys E to H after heat treatment. AAR Class C rail steel was used as the reference alloy. The AAR standard for Class C does not stipulate any requirements for the yield strength properties. Alloys E to F had a yield strength ranging from 714-829 MPa. The tensile strength for AAR Class C is required to be >1050 MPa (Figure 8) and alloy F achieved a tensile strength of 1224 MPa while the other alloys had a lower tensile strength, alloy F also showed the highest yield strength. The hardness of alloys F is higher than the hardness range stipulated for the AAR Class C alloy in the rim. The elongation of alloys E to F is higher than the 7% stipulated for the AAR Class C alloy (Figure 9). The Alloy F showed the lowest elongation.

Table 4. Tensile properties (yield strength (YS), ultimate tensile strength (UTS), elongation, reduction in area (RA) of alloys E to H and AAR Class C (forged) rail wheel steels.

Alloy	0.2% YS (Mpa)	UTS (Mpa)	Elongation (%)	RIA (%)	Hardness (HV) average	Neutron Diffraction		Point Counting	
						% Retained austenite	BCC	M	B
E	722±18	919±29	13.7±0.88	20.0±5	284±6	2.6	97.4	12	88
F	829±9	1224±44	9.4±0.6	9.1±0.8	412±41	20	80	13	87
G	738±58	978±53	10.5±2.1	17.3±6.5	352±7	9.4	90.6	2	98
H	714±45	960±54	11.9±1.5	18.1±11.8	295±2	25.5	74.5	10	90
AAR Class C*	-	>1050	7 (min)	-	320-376 (Rim)	-	-		

**A. Kapito, J.Jonck and G. Maruma [39]*

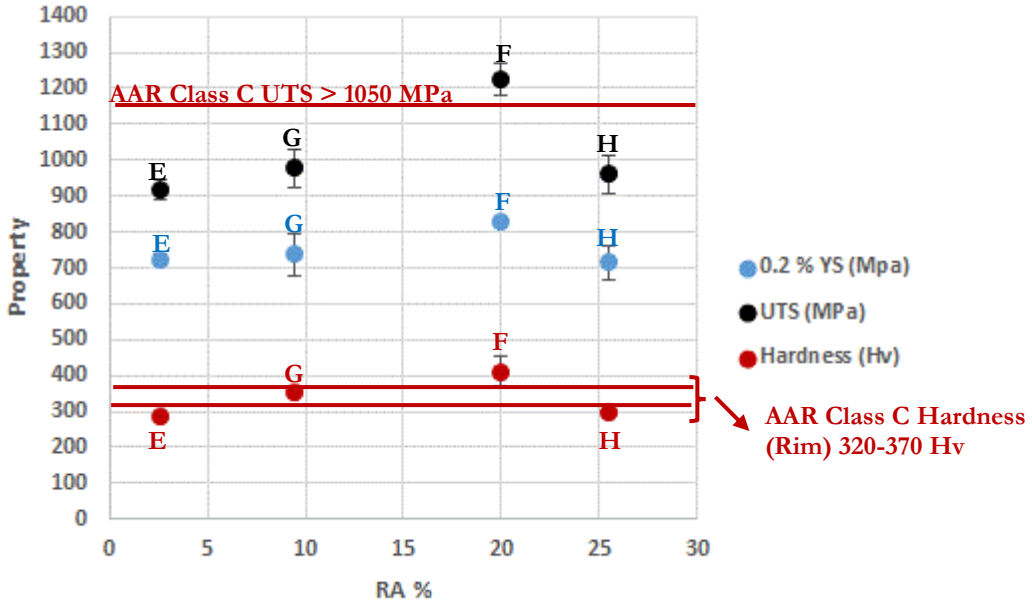

Figure 8. 0.2% yield (YS), ultimate tensile strength (UTS) and hardness versus retained austenite (%RA) results for Alloys E to G compared to AAR Class C alloy.

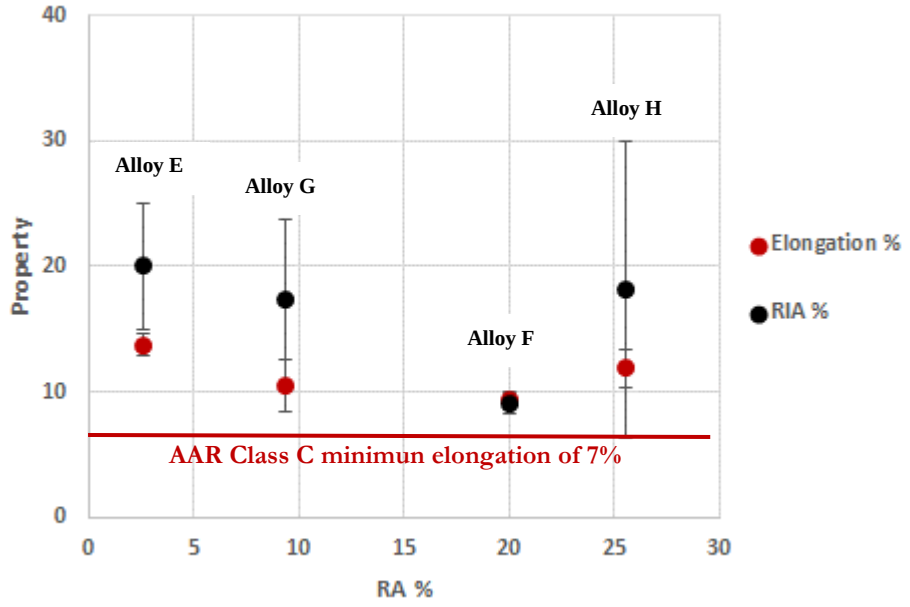

Figure 9. Elongation and reduction in area (RIA) versus retained austenite (%RA) results for alloys E to G compared to AAR Class C alloy.

Figure 10 shows that the carbide-free alloys H to G fall in the grade for advanced high strength steel (AHSS) on the elongation vs tensile strength graph for steels. Alloy E is not carbide-free as it showed carbides in the microstructure due to its low silicon content and is not included in the diagram. Alloys F-H show a combination of high strength and moderate ductility. The ductility is a result of the high amount of retained austenite. The high strength emanates from the combination of fine bainite and the transformation induced plasticity (TRIP) effect. The TRIP effect occurs due to the formation of strain induced martensite during tensile testing, increasing the tensile strength of the steel.

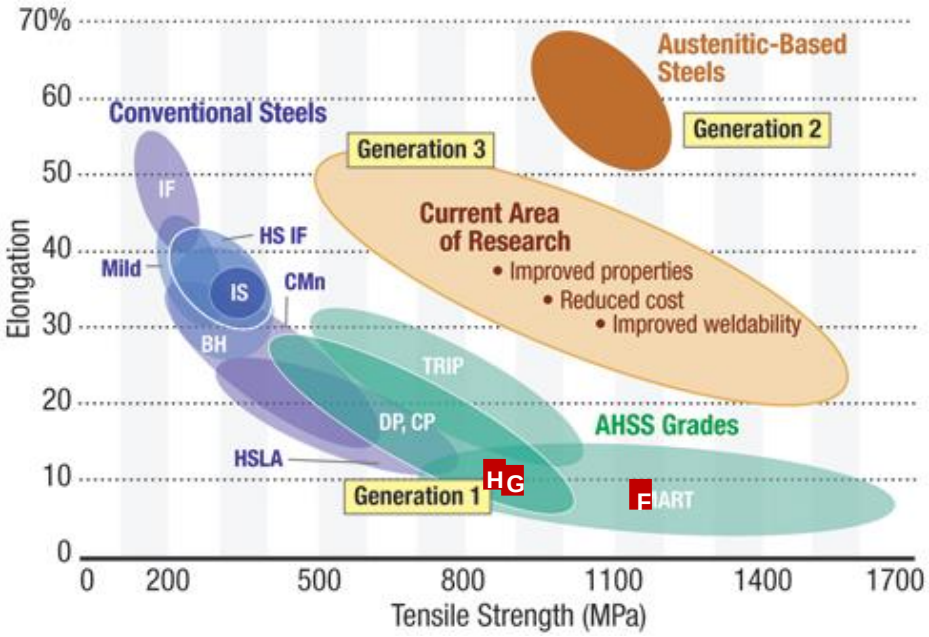

Figure 10. Elongation (%) vs tensile strength (MPa) data for conventional, advanced high strength and austenitic-based steels. The current area of research is also shown for the development of new generation steels [40].

4.6. Charpy V-Notch Impact Testing.

Research has found that high toughness results in a steel with a high resistance to crack initiation and propagation during rolling contact fatigue [8][22][31]. The results for the charpy v-notch impact testing conducted on alloys E to H are given in Figure 11. Alloys E and F show the lowest impact energy absorbed, followed by Alloy G. Alloy H shows the highest impact energy absorbed. Alloys E, F and G show a low impact energy of ≤ 5J up to 100°C, whilst Alloy H shows an impact energy of about 6J up to 50°C, after which its impact energy increases drastically. The ductile to brittle transition temperature (DBTT) for Alloys E, F and G is at high temperatures > 120°C, but Alloy H has a DBTT at about 80°C. Samples from AAR Class C wheel alloy, in the rim, were tested at room temperature and the results are shown in Table 5. Alloy H showed similar energy absorbed at room temperature as AAR Class C. Alloy H has the highest retained austenite of 25% and, from previous results, showed the highest elongation and reduction in area but lowest hardness. The bainitic alloys F and H although containing high retained austenite contents, showed low CVN values, due to the formation of brittle martensite during impact testing.

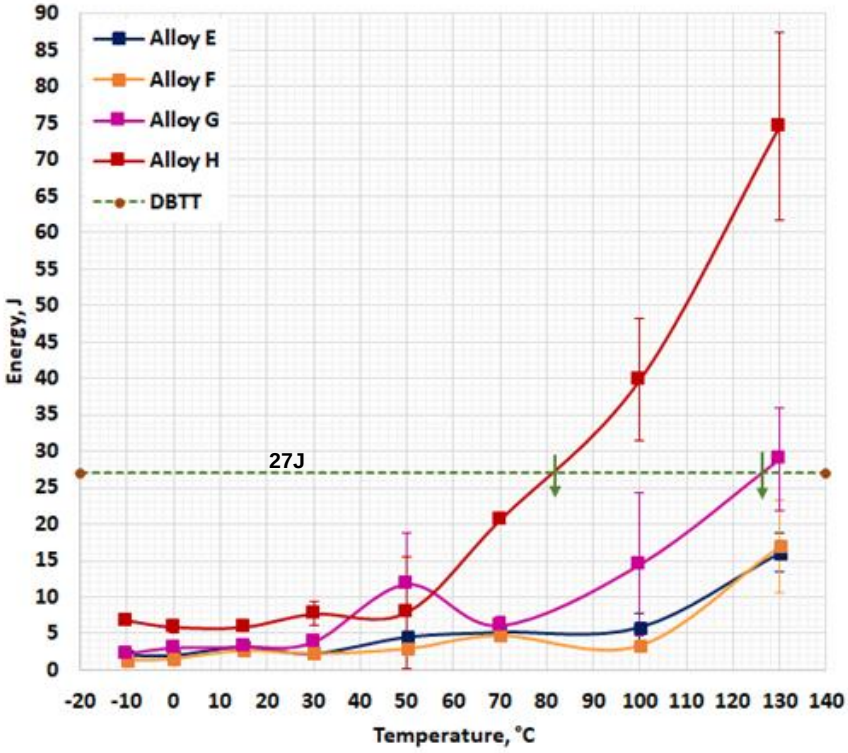

Figure 11. Impact toughness results for Alloys E to H, showing the ductile to brittle transition temperature (DBTT) calculated at 27J.

Table 5. Impact Properties of alloys E to H and AAR Class C at room temperature (RT).

Alloy	*Average Impact energy absorbed at room temperature (J)*	*Retained Austenite*
AAR Class C Forged Wheel	*6.6**	-
Alloy E	*2.3±0.4*	*2.6*
Alloy F	*2.3±0.5*	*20*
Alloy G	*3.8±0.6*	*9.4*
Alloy H	*7.7 ±0.7*	*25.5*

**A. Kapito, J.Jonck and G. Maruma [39]*

5. Discussion

The carbide-free bainitic alloys show beneficial mechanical properties of rail wheel applications. These properties however have been tested on 15mm thick laboratory samples. To transfer the beneficial properties of the carbide-free to actual wheel samples, with a thickness of about 130mm, heat treatment will need to be tailored for the alloys. The carbide-free alloys also contain martensite and the tolerable amount in thick rail wheels needs to be determined to avoid crack initiation during continuous rolling. The carbide-free alloys also have a high retained austenite which can transform to brittle martensite during operation. The amount of retained austenite also needs to be tailored.

6. Conclusions

Transmission Kikuchi diffraction analysis revealed cementite in the microstructure of alloy E with 0.36 wt% silicon, which was produced as a reference alloy. This alloy thus was not carbide-free. Carbide-free bainite was formed using common alloying elements used to produce steels but with a high silicon content >1 wt% in alloys F-G. The carbide-free alloys showed a mixed microstructure of martensite, bainite and retained austenite. The carbide-free alloys had an elongation > 7 % and Alloy F showed a UTS >1050MPa. The impact energy results showed that alloy H with the higher retained austenite of 25% showed better impact properties. The experimental alloys studied in this project generally showed poor impact properties.

7. Acknowledgement

We would like to thank the following people and organisations, without which this study would not have been possible: the University of Pretoria for providing technical support and academic supervision, Mintek, for technical and financial support, The Department of Science and Technology (DST), Advanced Materials Initiative (AMI)-Ferrous Metals Development Network (FMDN) for their financial support, the Nelson Mandela University, Department of Physics and Centre for HRTEM for transmission kikuchi diffraction (TKD) analysis and the Nuclear Energy Council for South Africa (NECSA) for their neutron diffraction analysis.

8. References

[1] N. Ridley, A Review of the Data on the Interlamellar Spacing of Pearlite, Metallurgical Transactions A Volume 15a, June 1984, pp. 1019-1036

[2] B. Bramfitt, *A Metallurgical Perspective of the Role of Rail Steel in the Growth of America*, 2011 AIST Adolf Martens Memorial Steel Lecture, A Publication of the Association for Iron & Steel Technology, January 2012, pp. 158-172

[3] https://www.scribd.com/document/355255964/ihha-guidelines-to-best-practices-for-heavy-haul-railways-operations-wheel-rail-interface-issues-pdf, cited November 2016

[4] M Diener and A Ghidini, *Materials for Heavy Haul Solid Wheels: New Experiences*, Special Issue Paper, Proc. IMechE Vol. 224 Part F: J. Rail and Rapid Transit, JRRT356, 19 April 2010, 421-428

[5] ASM International, *High-Carbon Steels: Fully Pearlitic Microstructures and Applications*, cited August 2015 2005 ASM International, Steels: Processing, Structure, and Performance (#05140G), ASM International, Materials Park, Ohio, USA, pp. 281-295

[6] W.E. Stumpf, *Phase Transformations in Metals and their Alloys*, The University of Pretoria, Materials and Metallurgical Engineering, Course NFM 700, 2010

[7] G. Vander Voort, The Interlamellar Spacing of Pearlite, April 9, 2015 https://vacaero.com/information-resources/metallography-with-george-vander-voort/1437-the-interlamellar-spacing-of-pearlite.html, cited September 2017

[8] G. Gersh and R. Heyder, *Advanced Pearlitic and Bainitic High Strength Rails Promise to Improve Rolling Contact Fatigue Resistance*, https://www.researchgate.net/publication/266035565_Advanced_pearlitic_and_bainitic_high_strength_rails_promise_to_improve_rolling_contact_fatigue_resistance, cited June 2017

[9] A. Gianni, A. Ghidini and A. Ekberg, *Bainitic Steel Grade for Solid Wheel: Metallurgical, Mechanical and In-Service Testing*, Proc, IMechE Vol. 223 Part F: J. Rail and Rapid Transit, pp 163-171, www.ndt.net, cited 28 September 2014.
[10] http://www.transnetfreightrail-tfr.net/MDS/Pages/Overview.aspx, cited November 2016
[11] H.K.D.H. Bhadeshia, *New Bainitic Steels by Design*, University of Cambridge, University of Cambridge, www.msm.cam.ac.uk/phase-trans, cited June 2013
[12] H.K.D.H. Bhadeshia and D. V. Edmonds, *The Bainite Transformation in a Silicon Steel*, Metallurgical Transactions A, Volume 10A, July 1979, pp. 895-907
[13] B.P.J. Sandvik, *The Bainite Reaction in Fe-Si-C Alloys: The Primary Stage*, Metallurgical Transaction A, Volume 13A, May 1982, pp. 777-787
[14] J. Cornide, C. Garcia-Mateo, C. Capdevila and F.G. Caballero, *An Assessment of the Contributing Factors to the Nanoscale Structural Refinement of Advanced Bainitic Steels*, Journal of Alloys and Compounds 577S (2013) S43–S47
[15] H. Amel-Farzad, H.R. Faridi, F. Rajabpour, A. Abolhasani, Sh. Kazemi and Y. Khaledzadeh, *Developing Very Hard Nanostructured Bainitic Steel*, Materials Science and Engineering A559 (2013) 68-73
[16] F.G. Caballero, M.K, Miller, S.S. Babu and C. Garcia-Mateo, *Atomic Observations of Bainite Transformation in a High Carbon High Silicon Steel*, Acta Materialia 55 (2007) 381-390
[17] C. Lonsdale and D. Stone, *Some Possible Alternatives for Longer-Life Locomotive Wheels*, Proceedings of IMECE02, 2002 ASME International mechanical Engineering Congress & Exposition, November 17-22, New Orleans, Louisiana, pp. 239-244
[18] F.C. Zhang, B. Lv, C.L. Zheng, Q. Zou, M., Zhang, M. Li, and T.S. Wang, *Microstructure of the Worn Surfaces of a Bainitic Steel Railway Crossing*, Wear, 268, 2010, 1243-1249
[19] S. Ahmed and A. Zervos, *Railway Ballast*, Engineering and the Environment, University of Southampton, http://www.southampton.ac.uk/~muvis/case_studies/06_Railway_ballast.html, cited September 2014
[20] http://www.trackguy.com/trackwork_101.htm, cited September 2014
[21] R.P.B.J. Dollevoet, *Design of an Anti-Head Check Profile Based on Stress Relief*, PhD Thesis, University of Twente, Enschede, The Netherlands
[22] *Rolling Contact Fatigue: A Comprehensive Review*, DOT/FRA/ORD-11/24, Final Report November 2011, U.S. Department of Transportation, Federal Railroad Administration, Office of Railroad Policy and Development Washington, DC 20590, http://ntl.bts.gov/lib/43000/43400/43400/TR_Rolling_Contact_Fatigue_Comprehensive_Review_final.pdf, cited September 2014
[23] *Transport Safety Board of Canada*, Railway Investigation Report No. R11D0099, Non-Main-Track Derailment, Agence Métropolitaine de Transport, Commuter Train No. 805, Mile 73.84, Saint-Hyacinthe Subdivision, Montreal, Quebec, 09 December 2011, http://www.tsb.gc.ca/eng/rapports-reports/rail/2011/r11d0099/r11d0099.pdf, cited September 2014
[24] M.R. Zhang and H.C. Gu, *Microstructure and Properties of carbide Free Bainite Railway Wheels Produced by Programmed Quenching*, Materials Science and Technology, Vol. 23, No. 8, 2007, pp. 970-974
[25] *Fracture and Fatigue Damage Tolerance of Bainitic and Pearlitic Rail Steels*, Research Results, U.S Department of Transportation, Federal Railroad Administration, RR06-02, February 2006, www.fra.dot.gov/Elib/Document/2136, cited September 2014
[26] H.A. Aglan, Z.Y. Liu, M.F. Hassa and M. Fateh, *Mechanical and Fracture Behaviour of Bainitic Rail Steel*, Journal of materials Processing Technology, 151, 2004, 268-274.
[27] V.V. Pavlov, L.A. Godik, L.V. Korneva, N.A. Kozyrev and E.P. Kuznetsov, *Railroad Rails Made of Bainitic Steel*, Metallurgist, Vol.51, Nos 3-4, 2007, pp.209-212
[28] H.K.D.H. Bhadeshia and J. Vijay, *Improvements in and Relating to carbide-Free Bainitic Steels and Methods of Producing Such Steels*, Patent No. WO 96/22396, 25 July 1996

[29] H. Kageyama, M. Ueda and K. Sugino, *Process for Manufacturing High-Strength Bainitic Steel Rails with Excellent Rolling-Contact Fatigue Resistance*, Patent No. US 5382307, 17 January 1995
[30] M. Ueda, K. Uchino, K. Iwano and A. Kobayashi, *Bainite Type Rail Excellent in Surface Fatigue Damage Resistance and Wear Resistance*, Patent No. AU 737977 B2, 6 September 2001
[31] J. Jaiswal, P. Sécordel and F. Fau, *Corus Premium Grades to Adress Wear And Rolling Contact Fatigue*,
https://www.arema.org/files/library/2010_Conference_Proceedings/Corus_Premium_Grades_to_address_Wear_and_Rolling_Contact_Fatigue.pdf, cited September 2014
[32] I. Poscmann, E. Tschapowetz and H. Rinnhofer, *Heat Treatment Process and Facility for Railway Wheels, Tyres and Rings*, Advanced Forging Technologies, www.werkstoff-service.de, accessed 12 April 2014.
[33] R. Zhou, Y. Jiang, D. Lu, R. Zhou and Z. Li, *Development and Characterization of a Wear Resistant Bainite/Martensite Ductile Iron by Combination of Alloying and a Controlled Cooling Heat-Treatment*, Wear, 250, 2001, 529-534.
[34] CQU, http://www.cre.cqu.edu.au/projects/rail_grinding.htm, cited 11 May 2014.
[35] R. Lewis and U.Olofsson, *Mapping Rail Wear Regimes and Transitions*, Wear 257 (2004) 721-729
[36] H.A. Aglan, and M. Fateh, *Fracture and Fatigue Crack Growth Analysis of Rail Steels*, Mechanics of Materials and Structures, Volume 2, No. 2, February 2007.
[37] S. Khare, K. Lee and H.K.D.H. Bhadeshia, *Carbide-Free Bainite: Compromise between Rate of Transformation and Properties*, Metallurgical and Materials Transactions A, Volume 41A, April 2010, pp. 922-928
[38] H.K.D.H. Bhadeshia, *Bainite in Steels*, Second Edition, Institute of Materials, March 2001, ISBN 1 86125 112 2 (H)
[39] A. Kapito, G. Maruma and J. Jonck, Metallurgical Characterisation of 34-Inch Advanced Casting Technique (ACT) Class B Cast and Forged Rail Wheel from Transnet Engineering Koedospoort, Mintek Internal Report No. 42228, 18 December 2015
[40] S. Keeler, The Science of Forming- Automotive Steels--Online Technical Resources, 1 May 2012, https://www.metalformingmagazine.com/enterprise-zones/article/?//2012/5/1/Automotive_Steels--Online_Technical_Resources, visited January 2019